CHAPTER 6

TOPOLOGY OPTIMIZATION OF FPSRS

6.1 Overview

The present chapter focuses on topology optimizing the FPSRS and its performance, underlining the crucial role of optimization in achieving the most efficient system for operation in the ideal environment. Initially, the optimal vertical height of the FPSRS (H) to length of the BRS (B) ratio for STC-based FPSRS is analysed and discussed. Following this, the HTC-based FPSRS undergoes a numerical analysis and is compared with the STC variant. The discussion then shifts to OTC-based FPSRS, which is also numerically analysed and simultaneously compared with both HTC and STC. Furthermore, the analysis of FPSRS was presented under extreme solar radiation conditions, such as during the Summer solstice (SS) and Winter solstice (WS). This overview encapsulates the chapter's aim to demonstrate the critical importance of optimizing FPSRS to enhance its performance across different environmental conditions, thus advancing the effectiveness of solar thermal energy solutions.

6.2 Effective height to bottom (H/B) ratio for FPSRS

The angular position of the FPTRs in the FPSRS significantly influences system performance, which largely depends on the H/B ratio as discussed in recent open literature as mentioned in Section 2.7. However present section delves into a numerical investigation using RTA on a STC-based FPSRS, analysing the impact of varying values of Φ on its optical performance. The value of Φ can be altered by adjusting the H/B ratio. Two extreme solar radiation conditions, SS and WS, have been selected to obtain the minimum and maximum possible values of H/B. The results are presented in terms of ray classification as discussed in Table 4.2. The following discussion outlines the steps undertaken with the RTA and discusses the results obtained.

The steps to determine the optimal value of H/B for a STC-based FPSRS is shown in Fig. 6.1. Initially, the process commences with the specification of geometric data pertinent to the STC based FPSRS, where the H/B input condition is defined. This foundational step ensures that variations in H and B dimensions are considered within pre-established constraints, facilitating a comprehensive evaluation of different H/B configurations. Subsequent to establishing geometric parameters, the analysis integrates solar radiation data corresponding to SS and WS solar radiation conditions. This inclusion is critical for assessing the influence of varying solar radiation extremes on identifying the most effective value of H/B, thereby accommodating seasonal variations in solar exposure and their impact on the system's performance.

The core of the methodology lies in RTS and it is starting with the projection of a single ray from the TIS. This step is iteratively executed for each ray and meticulously recording key data points such as the rays' intersection points on the reflector, their lengths, and the angles at which they intersect the reflector. Such detailed recording is instrumental in analysing the optical behaviour of the system under different geometric and solar radiation conditions. This rigorous process is replicated across a spectrum of different values of H/B, alongside varying solar radiation and geometric conditions, to ensure a thorough exploration of potential configurations. It considers 1800 number of rays incoming from the TIS and that number derived from comprehensive research indicating no substantial difference in the outcome beyond this value, as discussed in section 5.4.4. In a singular set of conditions, approximately 1800 rays are scrutinized, cumulating in a grand total of around 6, 48, 000 rays across all tests. This extensive data collection is pivotal for identifying the most advantageous and optimum value of H/B for the FPSRS, ensuring that the findings are robust and representative of a wide range of operational scenarios. The results obtained from a numerical study on the STC-based FPSRS, by modifying the different value of H/B under two extreme atmospheric conditions (SS & WS), are presented in the subsequent discussion.

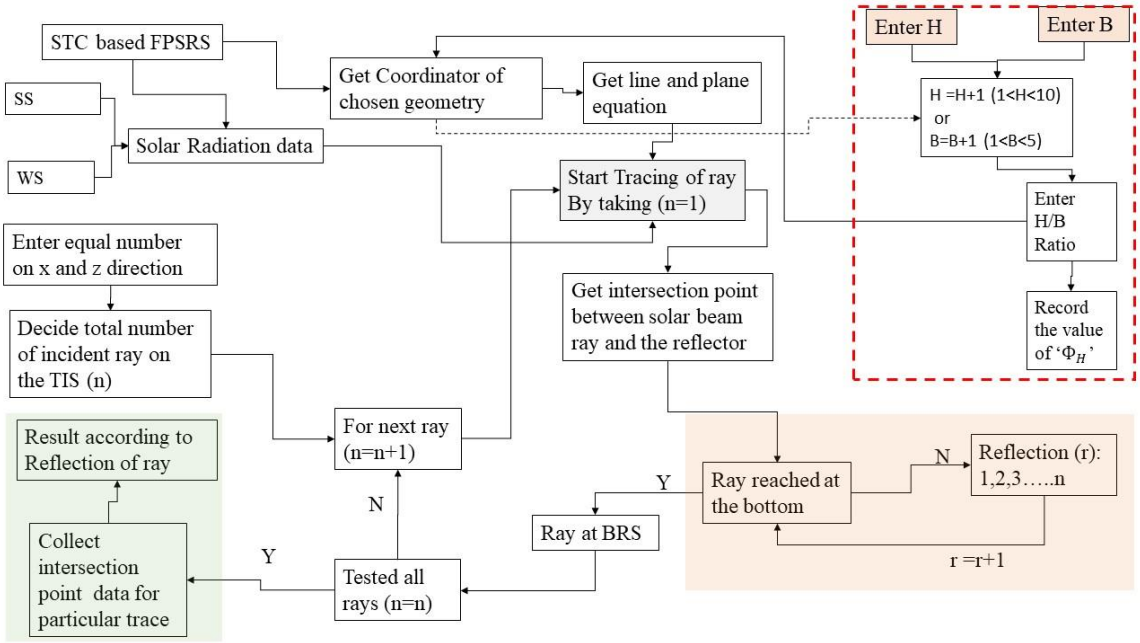

Fig. 6.1 Flowchart of for determining the optimal value of H/B in STC-based FPSRS

The input solar radiation data chosen for the study as SS day (21st June 2020) and WS day (21st December 2020) are displayed in Fig. 6.2 (a) and Fig. 6.2 (b), respectively. The figures only present a comparative analysis of the Direct normal irradiation (DNI) and Solar altitude angle (α_L). However, detailed numerical information on all other aspects is provided in Appendix D, in Table D.1.1 and

Table D.1.2 for the SS and WS conditions, respectively. The solar radiation data for the entire study were sourced from the web portal https://solcast.com/ (*Solcast*, 2020), operated and managed by the Australian company Solar and Storage Modelling Pty Ltd. The author received a virtual grant of USD 10,000 from the same company to collect the most recent solar statistics online, with the letter of grant approval presented in Fig. D.1 in Appendix D.

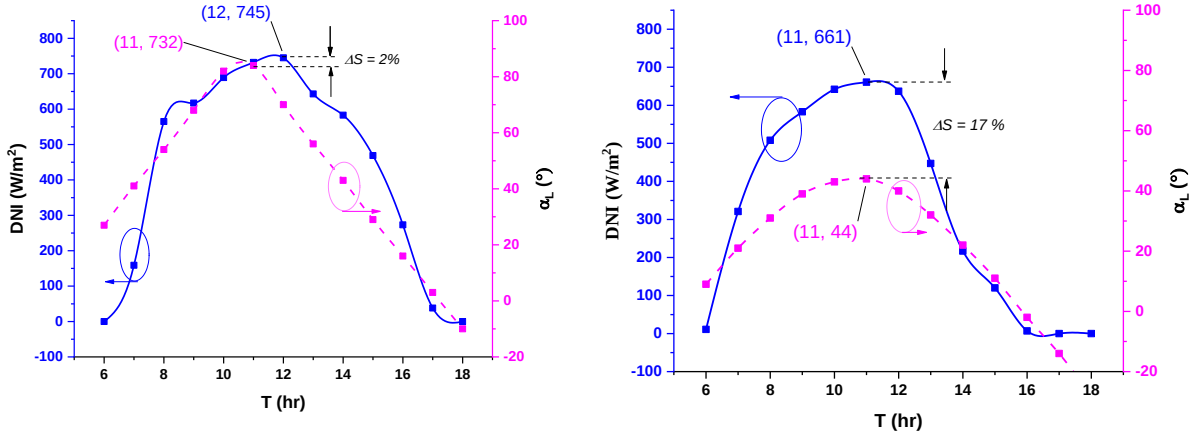

(a) (b)

Fig. 6.2 Solar irradiation data for (a) SS solar radiation condition (21st June 2020) and (b) WS solar radiation condition (21st December 2020) (*Solcast*, 2020)

It is observed that the variation in the value of DNI, as α_L changes, is relatively modest under SS compared to WS. Consequently, the peak values of DNI are nearly the same for both radiation conditions despite the varyingα_L. Due to this, in the WS condition, the solar system operates less effectively because of the comparatively lower value of α_L (Al-Maliki et al., 2023; Emamjome Kashan et al., 2023; X. Li et al., 2020). This information is essential for understanding the system's performance under different conditions. The difference in the solar radiation value (ΔS) is define as the ratio of the difference in the solar irradiation to the difference in the angle made by the ray to the surface and it can be compute by use of Eq. 6.1 (Emamjome Kashan et al., 2023). However, for the purposes of numerical calculations in this study, DNI is represented as I_{TIS} (incoming total irradiance on aperture area) and it is denoted as the amount of solar radiation carried by incoming rays.

$$\Delta S = \frac{\left(\frac{I_{\max}-I_{min}}{I_{\max}}\right)_{TIS}}{\frac{\alpha_{L\max}-\alpha_{L\min}}{\alpha_{L\max}}} * 100\% \qquad (6.1)$$

The RDP, as presented in Eq. (4.1), is used to determine the impact of radiation received on the BRS under different solar radiation conditions. The results are presented with considering various cases of rays as discussed and outlined in Table 4.2. The input condition for H/B has been considered

from H/B = 1 to 10 for both solar radiation conditions. Additionally, another condition with an H/B ratio of 1.52, which is the 'default condition' of the experimental setup as shown in Table 4.1, is considered and represented in as 'D' in Fig. 6.3. This brings the total number of H/B input conditions to eleven.

The results obtained for different value of H/B are depicted in Fig. 6.3 (a) for the SS solar radiation input condition and Fig. 6.3 (b) for the WS solar radiation condition. The RDP value is substantially more favourable when H/B is 2 for the SS as seen From Fig. 6.3 (a), while RDP exhibits extremely poor outcomes for an H/B of 10. However, there is a 4% variance observed in the case of E-type rays when H/B is varied from 2 to 1.52 (the default value). For an H/B of 1.52, the RDP value is significantly beneficial, showing just a 2.4% difference in the case of E-type rays when H/B fluctuates from 1 to 1.52 under the WS. Furthermore, the overall RDP profile is considered ideal when H/B is 2 and 1.52 for SS and WS conditions, respectively. Therefore, when the length of the base is 0.25 m, the optimal values for H will be 0.50 m and 0.38 m, and Φ will be 53° and 58° for SS and WS conditions, respectively.

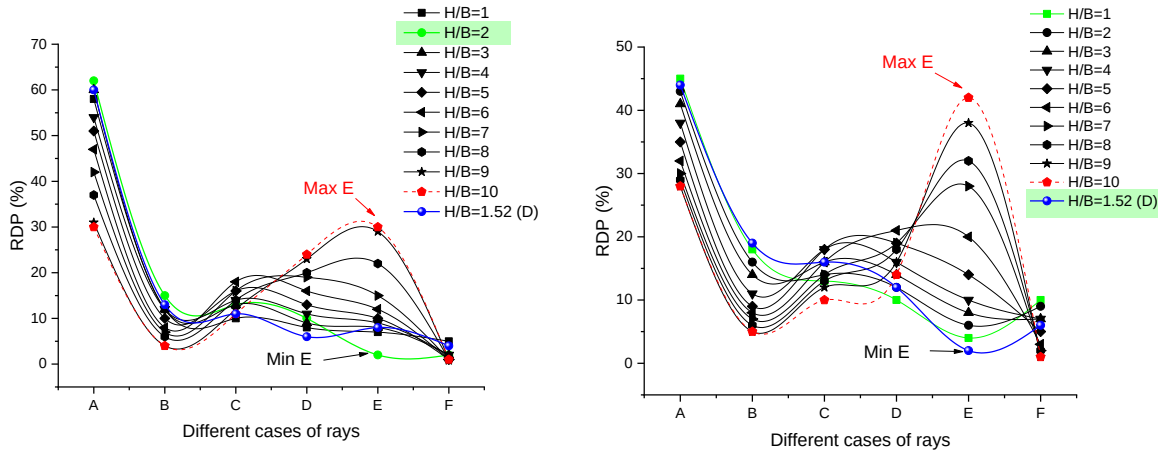

Fig. 6.3 Results of RDP for obtained the effective H/B in (a) SS and (b) WS, solar radiation condition.

The primary objective of this section is to evaluate the optical capabilities of a FPSRS having STC and having the best possible value of H/B or Φ. Analysing the RDP at the BRS for two extreme solar radiation conditions can help to get the best possible range of H/B for the maximum performance of the system. The findings suggest that the average RDP is at its best in SS when H/B is 2, but the RDP is at its best in WS when H/B is 1.52. Moreover, the value of Φ for the SS and WS solar radiation condition is 53° and 58°, respectively. However, in the next section, the best possible configuration ranging from STC to HTC and HTC to OTC are discussed.

6.3 Analysis of FPSRS having different configurations

The different configurations of FPSRS significantly influence the reflection pattern of solar radiation onto the receiving surface. The main objective of the present section is to discuss the impact of three different types of FPSRS configurations, namely the STC, HTC, and OTC with help of the numerical investigation to understand the optical performance of the system. Next, the experimental results of the STC-based FPSRS as presented in Chapter 4 are validated with the numerical results obtained for the similar kind of model. Later, the obtained results from all configurations are compared to determine the best possible configuration for different solar radiation conditions for optimal choice. Finally, the best chosen configuration has been analysed for different locations in India.

6.3.1 Validation of FPSRS having STC

Present section discusses the validation of experimental results of the STC-based FPSRS, as presented in Chapter 4 with numerical results for a similar model to better understand the viability of RTA. Later, the RTA is used to numerically analyse different configurations, specifically HTC and OTC. The mathematical and numerical models of the FPSRS with STC are explained in Chapters 3 and 5, respectively. The experiment of the STC-based FPSRS is discussed with obtained results in Chapter 4. The RTA used to numerically analyse the STC-based FPSRS is shown in Fig. 5.3 and discussed in detail in Section 5.3. The value of N_{TIS} is chosen as 1800 as discussed in Section 5.4. A similar study is presented in Section C.2 in Appendix C.

The validation of the RTA was conducted through experimental work performed by J. Patel et al. (J. Patel et al., 2023) on the STC based FPSRS. To ensure a meaningful comparative study, certain assumptions were made in line with the experimental investigation. Specifically, the value of N_{TIS} was set to 576. The input solar radiation value corresponded to as shown in Fig. 6.2 (a). The comparative results of two key parameters namely, the RDP and η_{opt} as computed with use of Eq. (4.1) and Eq. (3.17) and the obtained validation results were presented in Fig. 6.4 (a) and Fig. 6.4 (b), respectively. The analysis of the results revealed a slight difference of 2.9% in the case of RDP and the same was 3.2% in the case of η_{opt}. It is important to note that a significant portion of the observed variation in the results could be attributed to mechanical measurements and potential human errors while taking readings during the experiments. Based on these findings, it can be determined that the validation results are well-controlled, and the RTA demonstrates fairly good accuracy and reliability. Consequently, the developed RTA model can be confidently employed for evaluating other configuration based FPSRSs.

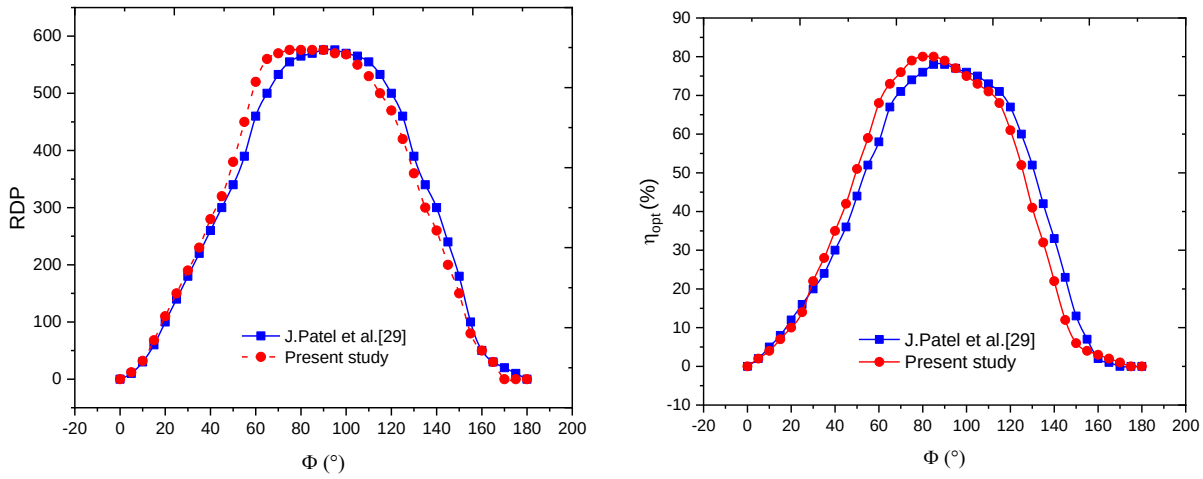

(a) (b)

Fig. 6.4 Validation of RTA with results of experimental work in the term of (a) RDP and (b) η_{opt}.

6.3.2 Numerical modelling of HTC and OTC based FPSRS

The numerical modelling of FPSRS equipped with HTC and OTC are detailed in the present section. The primary aim of the numerical modelling is to analyse the trajectory of ray from the moment it get entered the system at the TIS until, it reached to the BRS or exit the system from the TIS. The assumptions applied to calculate the ray behaviour are consistent with those discussed for the STC-based FPSRS model in Section 3.3.

First, the numerical model of the HTC-based FPSRS is presented. This model facilitates the analysis of the path followed by the ray after reflection from the reflector, including the intersection points on the reflector. These details are obtained through the use of two distinct coordinate systems: (i) the global coordinate system, which is considered the origin of the FPSRS, and (ii) the local coordinate system, which is applied at each intersection point between the ray and the corresponding reflector. The numerical model of HTC based FPSRS is presented in Fig. 6.5. Additionally, the front view give information about the path travelled by the ray to reach the BRS. However it is failed to give the exact information about the participating the reflector in the reflecting process and it will be get with help of and the top view. The R1, R2, R3, R4, R5, and R6 denote the number of reflectors constituting the HTC. The TIS coordinates are marked as A, B, C, D, E, and F, while those for the BRS are labelled W, X, Y, and Z.

All intersecting points are measured from a global coordinate of the system, represented as (0, 0, 0). It also details the application of the various angular terminologies used to predict the intersection points between the reflected ray and the reflector. Moreover, it is observed that as the number of reflections made by the ray increases, the concentration of energy in the ray is reduced,

which can be seen by the fading colour of the reflected ray. In the present model, the ray is reflected a total of three times before reaching the BRS. The three intersection points are also shown in the fig. 6.5 for better understanding.

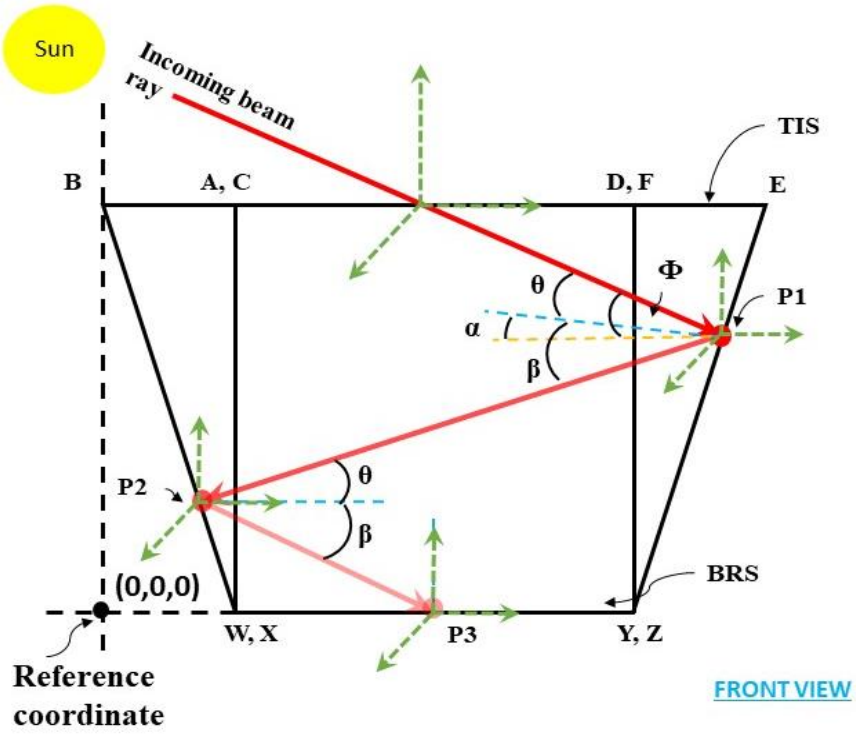

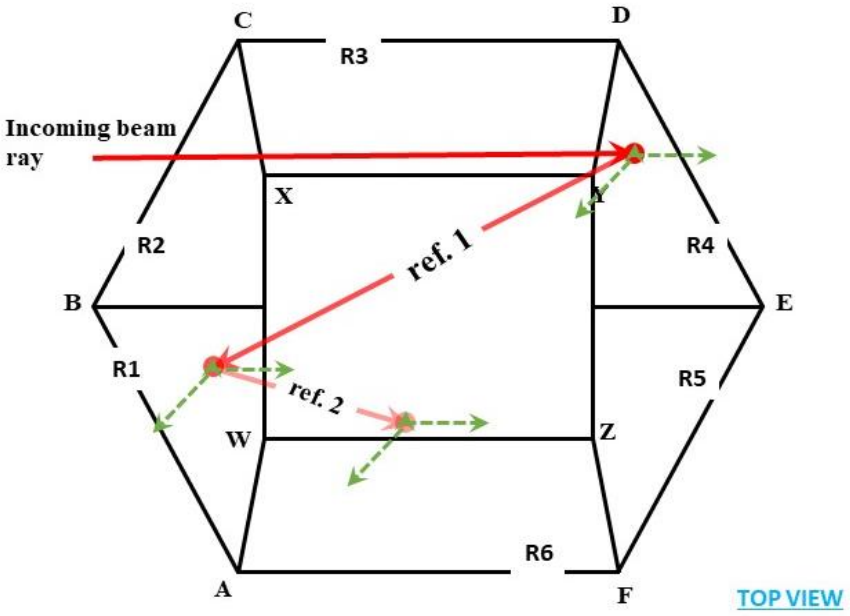

P1 : (x_1, y_1, z_1); P2 : (x_2, y_2, z_2); P3 : (x_3, y_3, z_3)

P1, P2, P3 : intersecting points

ref : reflecting ray

W, X, Y, Z : Coordinate points of BRS

A,B,C,D,E,F : Coordinate points of TIS

: Normal to plane

: Direction of Coordinate

: Direction of ray

: Boundary of reflector

Fig. 6.5 Numerical model of HTC based FPSRS

A similar numerical model is depicted in Fig. 6.6 for the OTC-based FPSRS. A clearer comprehension of the configuration and the possible role of the ray in the reflection process is made possible by the depiction of the opposite and neighbouring reflectors in the figure. The letters A, B, C, D, E, F, G, and H represent the coordinates of the TIS, while B1, B2, B3, and B4 denote the coordinates of the BRS. The ray that originates from the TIS and travels via two successive reflections from opposing reflectors before arriving at the BRS, is also explained by the model. However, the isometric view is sufficient for understanding the path followed by the ray to reach the BRS. Additionally, the significance of the angle θ is highlighted in Fig. 6.6 to illustrate its importance in determining the ray's next position and the subsequent intersection with the reflector.

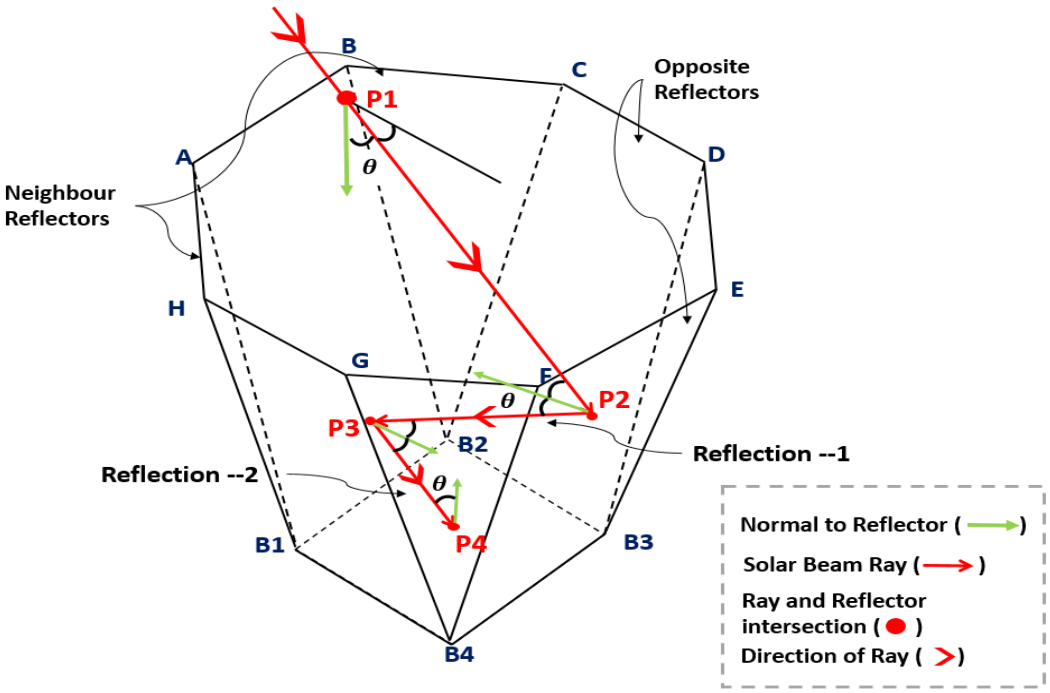

Fig. 6.6 Numerical model of OTC based FPSRS

Moreover, the path followed by the ray depends on the location, the involvement of either opposite or neighbouring reflectors, the angle made by the ray with the normal to the plane and Φ. In the present study, the value of Φ was set at a constant 60° (Wassie et al., 2022), and the impact of the opposite and neighbouring reflectors, among other parameters, on the ray's path is illustrated in Fig. 6.7 (a) for STC-based FPSRS, Fig. 6.7 (b) for HTC-based FPSRS and Fig. 6.6 for OTC-based FPSRS. The isometric view helps in understanding the physical principles behind the participation of different reflectors in determining the path followed by the rays. Where, the 'P_{OR}' and 'P_{NR}' indicate the locations of the intersecting points between the ray and the reflector when the ray's reflection is caused by the participation of opposite reflectors and neighbour reflectors, respectively. Besides, it is

evident that the path of the ray is significantly influenced by the nature of reflectors participation (R1 to R6) in the reflection process. Two types of reflections from the reflector were observed: (a) reflections from opposite reflectors and (b) reflections from neighbouring reflectors. When the reflection occurs due to opposite reflectors, the path followed by the ray is straightforward, and a substantial amount of energy reaches the BRS.

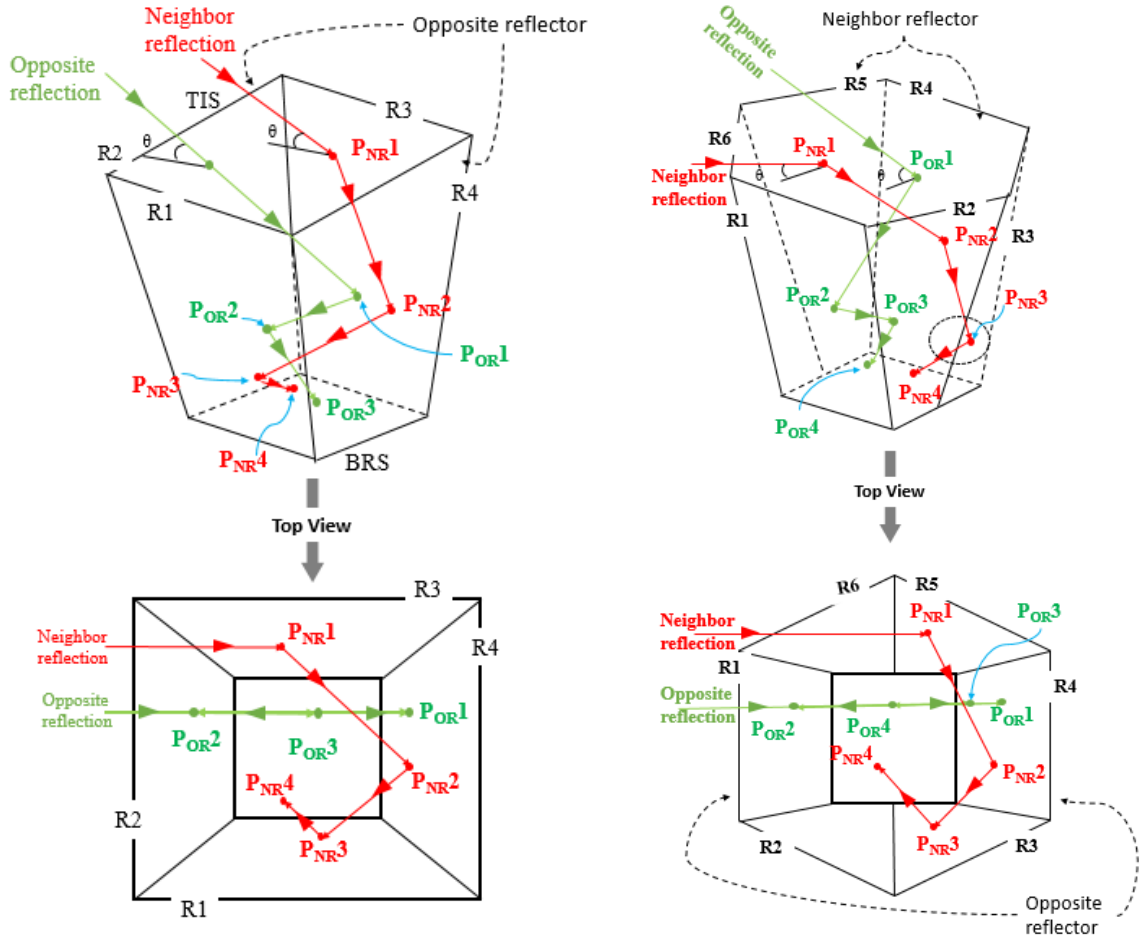

(a) (b)

Fig. 6.7 The path followed by the ray when reflected from opposite and via neighbour reflectors in the cases of (a) STC and (b) HTC, based FPSRS

Fig. 6.7 (a) illustrates the ray path traced considering the participation of opposite reflectors can be read as: TIS→R4→R2→BRS for STC -based FPSRS. However, the same in the case of HTC -based FPSRS, the ray follows the path: TIS→R4→R1→R4→BRS, as shown in Fig. 6.7 (b). It is essential to note that the ray path becomes complicated, lengthy, and reflective when neighbour reflectors play a significant role in the reflection process. For STC area, the ray path traced considering neighbour reflectors' participation is: TIS→R3→R4→R1→BRS (refer Fig. 6.7 (a)), and the same for HTC area it is TIS→R5→R4→R3→BRS (refer Fig. 6.7 (b)). The top view of both figures provides a better understanding of the path traced. Additionally, the path follow by the ray to

reach BRS while reflecting from the opposite and neighbour reflectors for OTC based FPSRS is presented in Fig. 6.8. The ray path traced considering neighbour reflectors' participation is: TIS→R3→R4→R7→BRS, and the same for opposite reflectors' participation is: TIS→R5→R1 →BRS (refer Fig. 6. 8).

Overall, it is observed that the ray path, when traced through neighbouring reflectors, becomes lengthy and involves multiple reflections, resulting in significant energy loss before reaching the BRS. However, understanding the behaviour of the rays from Fig. 6.8 is challenging especially in the case of OTC based FPSRS or FPSRS having multiple reflectors. Therefore, an isometric CAD model is presented in Appendix B to illustrate a similar scenario involving opposite and neighbouring reflections, aiding in comprehending the ray reflection and its involvement. Figs. B.2.1 and B.2.2 in Appendix B depict the ray's trajectory and path tracing process in the case of OTC-FPSRS. Additionally, the discussion further elaborates on the marching direction on TIS and presents CAD models of HTC and OTC-based FPSRS for better understanding. This detailed examination of ray behaviour and reflection paths enhances our understanding of the energy transfer dynamics within the solar system, offering valuable insights for optimizing solar energy collection and utilization in practical applications. The marching direction on TIS and the CAD models of the HTC and OTC-based FPSRS have been discussed in the following sections for better comprehension.

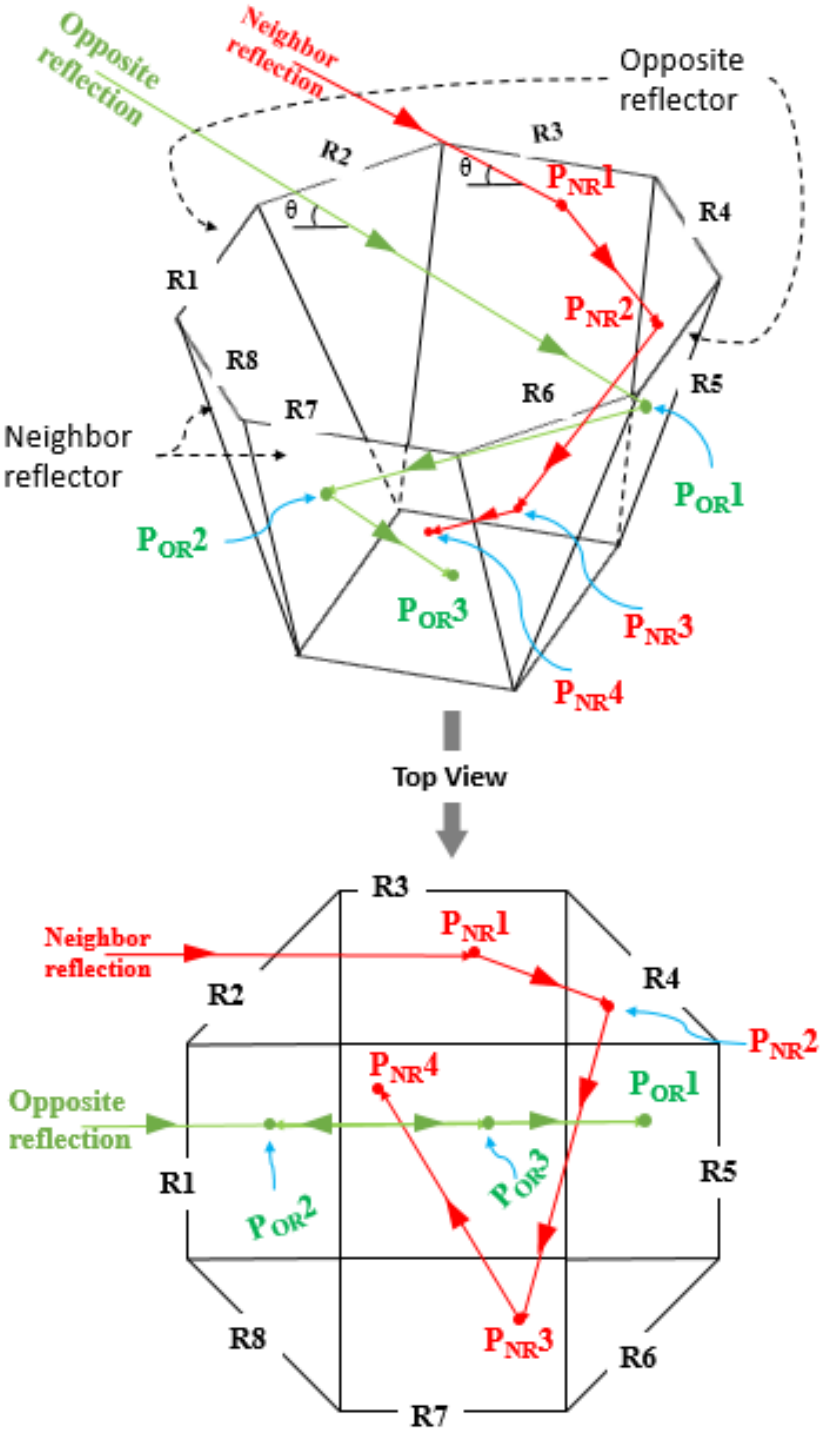

Fig. 6.8 The path followed by the ray when reflected from opposite and via neighbour reflectors in the cases of OTC based FPSRS

6.3.3 CAD modelling of HTC and OTC based FPSRS

The present section discusses the initial CAD model for the HTC and OTC-based FPSRS used in numerical computations. Subsequently, it addresses the core point's marching direction on the TIS for the HTC-based FPSRS. Unlike the STC, the HTC-based FPSRS does not adopt the same

marching approach. In the HTC system, portions of the TIS receiving rays which participated in the RTS process, designated as Participating areas (PA). Conversely, the remaining portions of the TIS, from which rays do not participated in the RTS process, are termed Non-participating areas (NPA). This concept of PA and NPA also applies to the OTC-based system.

The CAD models for the HTC-based FPSRS and the OTC-based FPSRS are illustrated in Figs. 6.9 and 6.10, respectively with representing the difference between PA and NPA on the TIS for both the configurations. The isometric view of the CAD models provides an overview of the entire geometry, as seen in Fig. 6.9 (a) for the HTC and Fig. 6.10 (a) for the OTC. The top view clarifies the distinction between PA and NPA in both configurations. Furthermore, the CAD models facilitate understanding the impact of PA and NPA on numerical computations. Notably, compared to the STC, the HTC and OTC-based FPSRS have smaller aperture areas but exhibit enhanced capability in redirecting case E and case F type of rays back to the BRS. This increased efficiency is attributed to their distinct features, including the unique configuration and arrangement of reflectors.

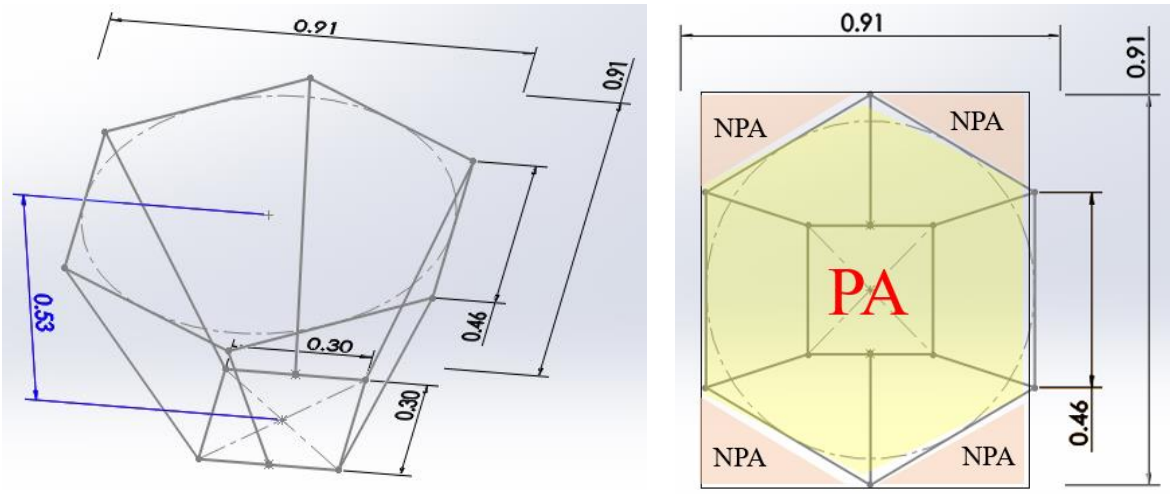

(a) (b)

Fig. 6.9 Representing the PA and NPA in the HTC based FPSRS (a) isometric view and (b) top view.

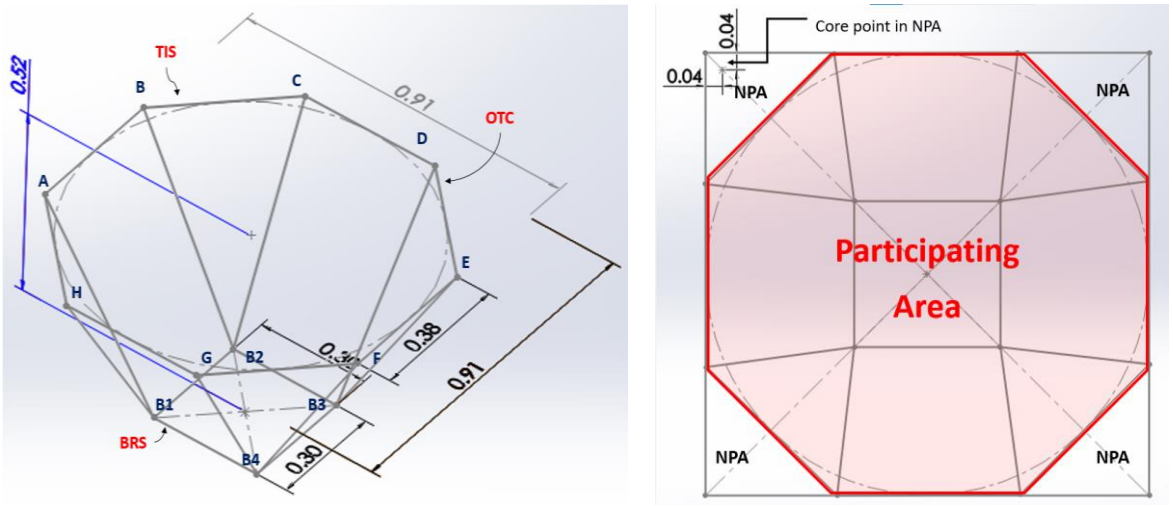

(a) (b)

Fig. 6.10 Representing the PA and NPA in the OTC based FPSRS (a) isometric view and (b) top view.

The default parameters or dimensions used for the numerical analysis of the HTC-based FPSRS and the OTC-based FPSRS are summarized in Tables 6.1 and 6.2, respectively. Notably, the NPA in HTC is 0.28 m^2 and it is 0.28 times than that of the STC-based FPSRS. However, the NPA value is reduced to 0.13 times in the case of the OTC, which is 46% less than that of the HTC. Although increasing the number of reflectors gradually decreases the NPA, it does not significantly improve the results and complicates the system's manufacturing. Therefore, in this study, the configuration is limited to the OTC, and no further analysis is conducted. Moreover, the dimensions used in the numerical analysis of the HTC-based FPSRS are derived from a prior experimental study on the STC-based FPSRS by authors (J. Patel et al., 2023).

Table 6.1 Default specifications of HTC based FPSRS used for numerical analysis

Parameter	**Specification**	**References**
A_{BRS} (m^2)	0.09	(J. Patel et al., 2023)
A_S (m^2)	0.83	(S. Wang et al., 2023)
H (m)	0.53	(J. Patel et al., 2023)
Length of single side of BRS (m)	0.30	(J. Patel et al., 2023)
Length of single side of HTC based TIS (m)	0.46	(J. Patel & Patel, 2023)
NPA (m^2)	0.28	--
PA (m^2)	0.55	(S. Wang et al., 2023)
Shape of the BRS (-)	Square	--
Shape of the TIS (-)	Hexagonal	--
Total no of reflectors (-)	6	--

Φ (°)	60	(J. Patel & Patel, 2023)

Table 6.2 Default specifications of OTC based FPSRS used for numerical analysis

Parameter	**Specification**	**References**
A_{BRS} (m^2)	0.09	(J. Patel et al., 2023)
A_S (m^2)	0.83	(S. Wang et al., 2023)
H (m)	0.53	(J. Patel et al., 2023)
Length of single side of BRS (m)	0.30	(J. Patel et al., 2023)
Length of single side of OTC based TIS (m)	0.38	(J. Patel & Patel, 2023)
NPA (m^2)	0.13	(S. Wang et al., 2023)
PA (m^2)	0.55	(S. Wang et al., 2023)
Shape of the BRS (-)	Square	--
Shape of the TIS (-)	Octagonal	--
Total no of reflectors	8	--
Φ (°)	60	(J. Patel & Patel, 2023)

The CAD model primarily provides information about the system's external geometry, whereas numerical modelling offers insights into the internal physics and the behaviour of rays. Numerical models also assist in understanding the underlying behaviour of different types of rays and their participation in the RTS process. The understanding of the rays' behaviour, including reflection patterns, pathways, and potential interactions with the reflector, the classification of rays into six different cases, as discussed in Table 4.2, is utilized for analysing the RDP on the BRS.

However, the information about the marching direction of the core points on the TIS in HTC and OTC differs from that in the case of STC. In HTC and OTC-based FPSRS, the PA and NPA are considered when choosing the marching direction on the TIS. However, there is no difference in the marching direction in the case of HTC and OTC. Therefore, in the present section, the marching direction for HTC-based FPSRS is sufficient for understanding the marching process in different configurations than STC. The marching direction of rays in the HTC-based FPSRS is presented in Fig. 6.11. Here, coordinates X_1, X_2, X_3, and X_4 cover the total area, including both NPA and PA regions. However, the PA is denoted by coordinates A, B, C, D, E, and F, which collectively form the HTC. The yellow line signifies the path of the solar beam ray, while the black line defines the system boundary. The green lines in the diagram represent the trajectories of the core points for numerical investigation, and the red lines define the boundary conditions of the HTC. Furthermore, the TIS coordinates represented by i, and j correspond to the core points coordinated along the x and y directions. The green-coloured line in the illustration indicates the direction of progression order for the RTA considered in the simulation.

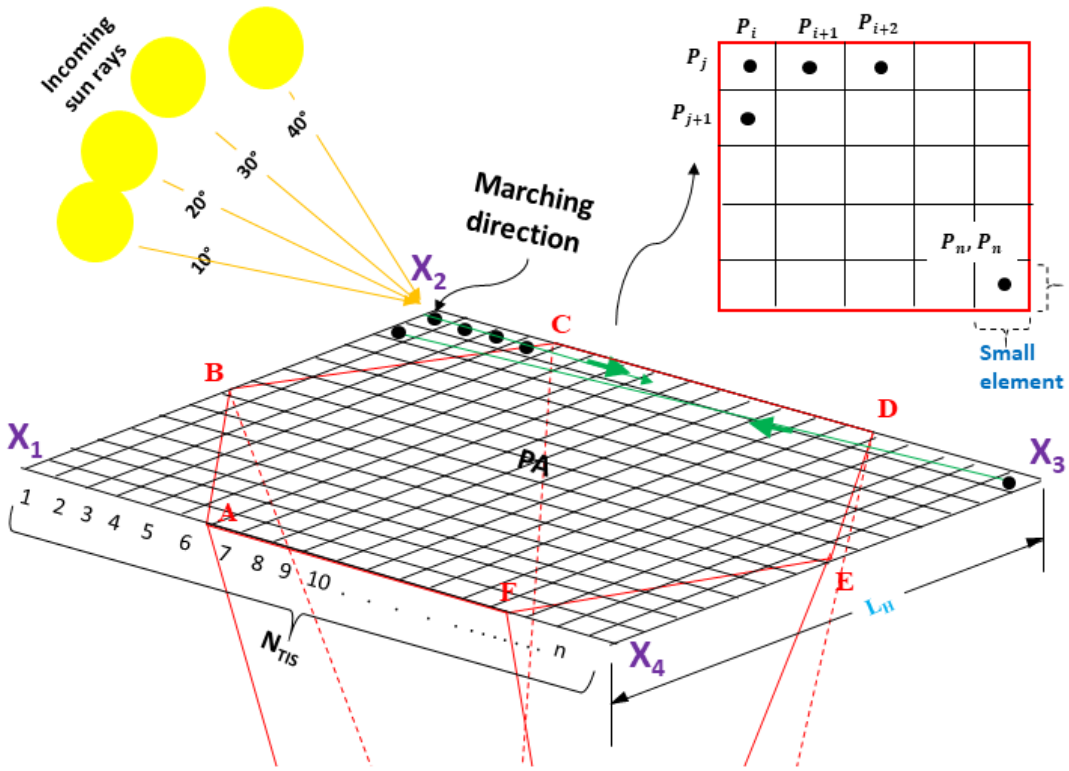

Fig. 6.11 Marching direction of the core point on the TIS of the HTC based FPSRS.

Next, a discretized approach is utilized to analyse the behaviour of a single ray on the TIS. The RTS process is executed using a similar RTA as shown in Fig. 5.3, and the same steps are employed in the simulation, as discussed in section 5.3. However, care has been taken when deciding the TIS configuration, such as HTC or OTC. Additionally, the numerical analysis considers various parameters such as incident angle, reflector geometry, and solar flux distribution. The differences in behaviour between HTC and OTC configurations are carefully examined to understand their respective performance characteristics. Moreover, the influence of different environmental conditions on the system's efficiency is investigated with providing valuable insights for optimizing the design. In the following discussion, the results obtained from the numerical analysis are presented and discussed for further clarification.

6.3.4 Comparative results

The present section discusses the results obtained from the numerical analysis conducted for the various configurations considered for the FPSRS. Firstly, the comparative behaviour of STC and HTC is presented with focusing on the results in terms of RDP. Following this, a comparison between

STC and OTC is made. Subsequently, the optimum configuration is determined for further investigation. Lastly, the best configuration is analysed for different territories in India, and the best possible results are discussed and presented.

The results of the behavioural pattern of ray after being reflected from the reflectors of FPSRS having STC and HTC are presented in Fig. 6.12. From the results it is observed that the case A type of rays shows that STC has favourable response in comparison to HTC, with the highest value of RDP is 69 %. When the value of θ is in the range of 60° to 120°, a steep slope is observed in case of both STC and HTC. Regarding case B type of rays the value of RDP for STC and HTC are nearly the same, when θ is ranging between 40° to 65° and 120° to 140° respectively. However, HTC shows a better RDP profile compared to STC for the range of $75°<\theta<120°$. This indicates that HTC performs better with case A type of rays.

A similar observation is noted for case C type of rays, but the RDP profile of STC does not show good results compared to HTC when θ is in the range of 15° to 40° and 140° to 165°. Yet, both types of configurations exhibit a similar RDP profile in the range of $40° < \theta < 140°$, and here too, HTC yields positive results compared to STC. The results of case D type of rays clearly indicate that HTC provide a better RDP than STC when the value of θ is between 40° to 140°. The results of RDP in the case of E and F types of rays are depicted in Fig. 6.12 (e) and Fig. 6.12 (f), respectively. In the case of E and F types of rays, RDP is considered as the number of rays that left the system from the TIS relative to the number of rays that entered the system from the TIS. From Fig. 6.12 (e), it is observed that the number of rays leaving the system is highest when the value of $0° < \theta < 40°$ and $140° < \theta < 180°$ for the case of E types of rays. Similarly, Fig. 6.12 (f) reveals that the number of rays leaving the system is highest when the value of $0° < \theta < 45°$ and $130° < \theta < 180°$ for the case of F types of rays. However, the overall observation suggests that HTC exhibits a better RDP than STC. This positively impacts the optical performance of the FPSRS. Therefore, the overall results of HTC are observed to be more favourable compared to STC for cases D, E, and F types of rays. In conclusion, it can be stated that HTC offers a better and optimum RDP for the BRS compared to STC.

Table 6.3 shows the comparative results between HTC and STC for the SS and WS two distinguished solar radiation condition. The results show that HTC performs better in specific scenarios due to a significantly smaller number of rays leaving the system, resulting in better RDP. However, the differences in results between STC and HTC for the case of WS were typically insignificant, especially for the case of D, E and F type of rays. Based on these findings, the HTC for FPSRS has greater strengths and may be selected for particular designs.

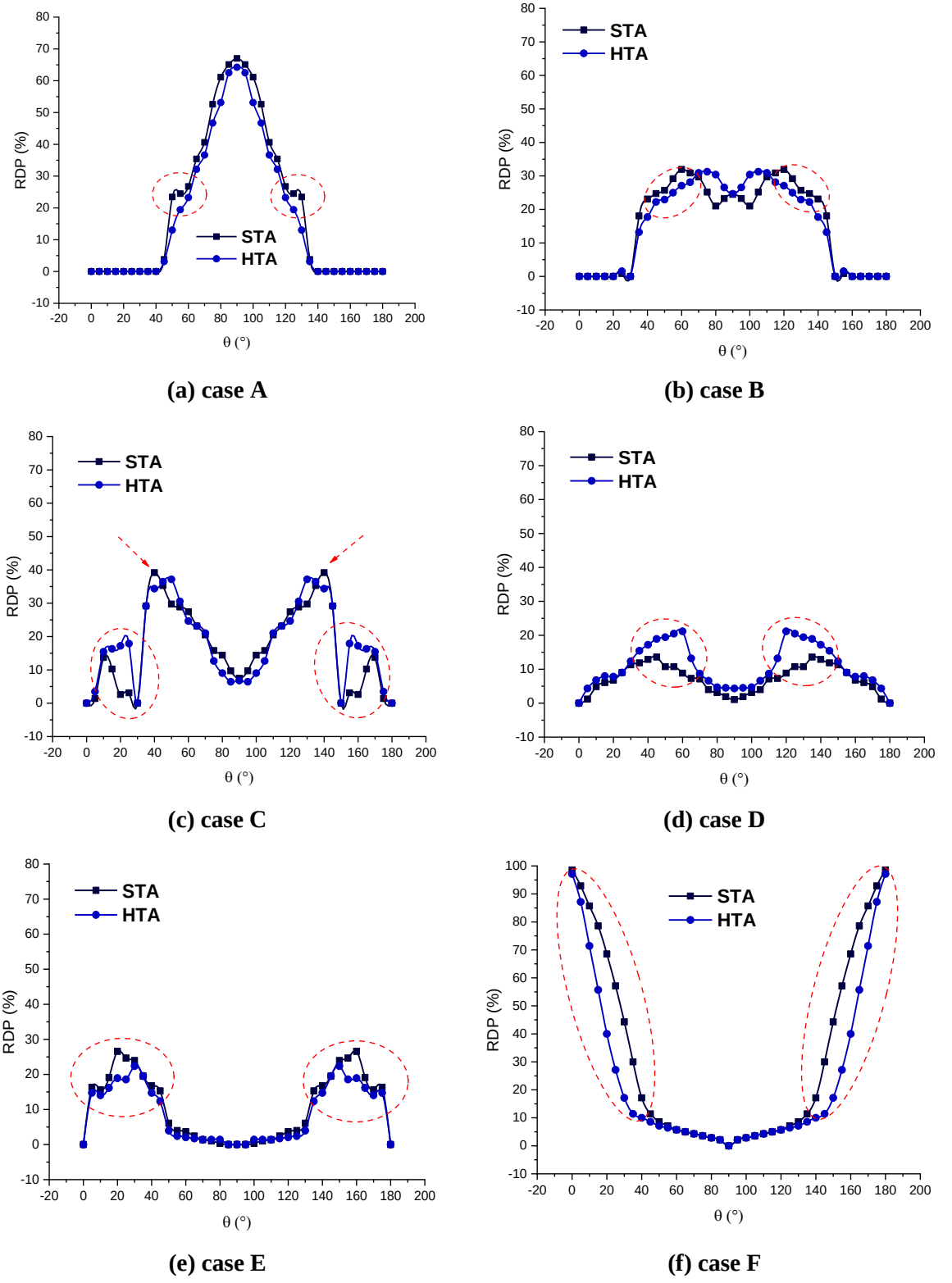

Fig. 6.12 Representation of the RDP for STC and HTC-based FPSRS for various values of θ as per the ray classification in Table 4.2.

Table 6.3 Comparative result of STC and HTC based FPSRS for SS and WS solar radiation condition.

Solar Data	**Type of ray**	**Results η_{opt}, range**	**Overall performance**	**Remark**
SS	Case A	STC > HTC by 6%, 40°< θ <60° & 150°< θ <170°	STC gave positive output	Overall HTC gave better RDP due lower number of rays leaving the system.
	Case B	HTC > STC by 8%, 65°< θ <105°	HTC gave positive output	
	Case C	HTC > STC by 12%, 15°< θ <40° & 115°< θ <140°	HTC gave positive output	
	Case D	HTC > STC by 9%, 35°< θ <125°	HTC gave positive output	
	Case E	STC > HTC by 13%, 15°< Φ <40° & 125°< Φ <140°	HTC gave positive output	
	Case F	STC > HTC by 18%, 0°< θ <40° & 140°< θ <180°	HTC gave positive output	
WS	Case A	STC > HTC by 3.2%, 25°< θ <45° & 135°< θ <155°	STC gave positive output	The HTC yielded superior RDP results at a lower value of θ. Yet, the minor deviation was observed for the case D, E and F type rays
	Case B	HTC > STC by 7%, 55°< θ <125°	HTC gave positive output	
	Case C	HTC > STC by 12%, 15°< θ <40° & 145°< θ <165°	HTC gave positive output	
	Case D	HTC > STC by 1.2%, 35°< θ <145°	HTC gave positive output	
	Case E	STC > HTC by 5.4%, 15°< θ <40° & 135°< θ <165°	HTC gave positive output	
	Case F	STC > HTC by 13%, 0°< θ <45° & 150°< θ <180°	HTC gave positive output	

The comparative optical performance of HTC and STC is presented in Figs. 6.13 (a) and (b) for the cases of SS and WS. From the results, it is observed that the average value of η_{opt} for HTC is 71% while the SS solar radiation condition and 60% when WS solar radiation condition. In contrast for STC, the η_{opt} is 58% for SS and 51% for WS solar radiation condition. In other words, the value of η_{opt} for HTC is 11% and 7% more than STC, while SS and WS solar radiation condition respectively, compared to STC. Notably, both configurations perform better in case of SS solar radiation condition compared to WS solar radiation condition. A critical analysis of the results reveals that the value of η_{opt} closely follows the available I_{TIS} between 12 PM to 4 PM in case of WS solar radiation condition. Interestingly, the advantage of the HTC can be observed during the period of 6 AM to 12 PM in the case of WS solar radiation condition. On the other hand in case of SS solar radiation condition the difference between HTC and STC is evident and emphasizing the benefits of using HTC based FPSRS for different solar thermal application applications.

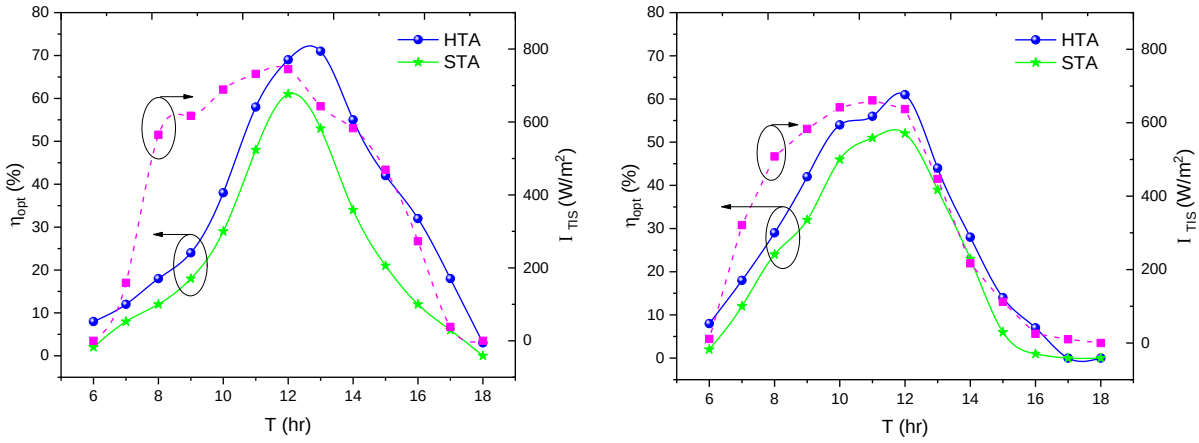

Fig. 6.13 Overall performance of FPSRS in (a) SS and (b) WS, solar radiation condition

Besides, the effects of I_{TIS} for the SS and WS solar radiation condition, on the RDP for HTC based system have been studied during the ideal sunrise to sunset time period (6 AM to 6 PM) as shown in Figs. 6.14 (a) and (b), respectively. The involvement of DR type of rays was found to be the largest in case of SS condition, reaching a maximum attainment value of RDP is 1350. However, in case of WS the maximum attainment of DR type of rays reduced to 960, showing a 28% decrease compared to SS conditions. Additionally, compared to WS scenarios, SS conditions showed a larger participation of SR and TR type of rays, with contributions of 12% and 10%, respectively. Additionally, the study discovered that the LR and THR type rays contributions were 8.2% and 11.2%, respectively under SS conditions and they were different in WS as well as it had a detrimental

influence on the optical performance of the SFPRS. Overall the RDP for HTC showed a positive impact in both SS and WS conditions, but SS exhibited better performance.

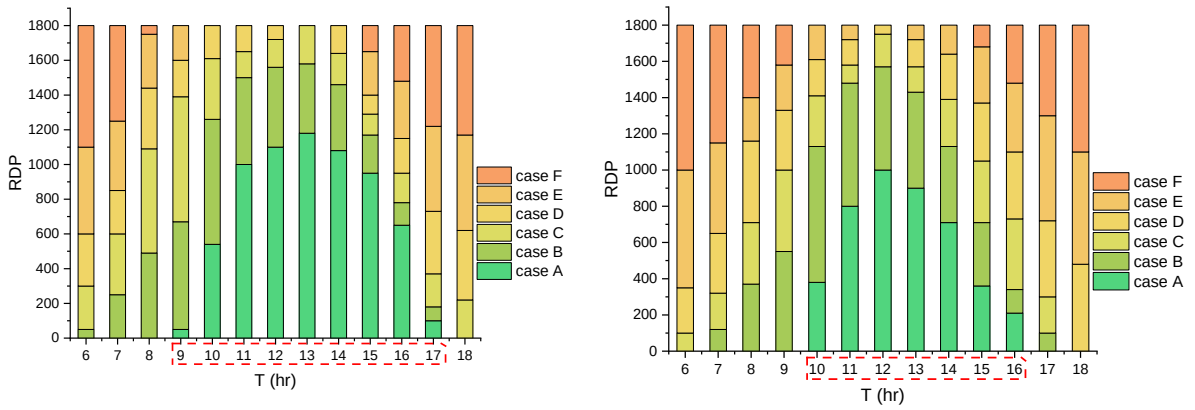

(a) (b)

Fig. 6.14 RDP for the different classification of the rays under (a) SS and (b) WS, solar radiation condition for HTC based FPSRS

Overall from the numerical investigation done on the configuration of HTC and STC based FPSRS. The obtained results of RDP and η_{opt} for two different solar radiation condition named SS and WS the interesting fact to know that the $\eta_{opt}$of the HTC was HTC was superior to the STC system. The greater involvement of case A and case B type of rays were the main factor for the HTC to enhance its efficiency. The importance of θ and the sun's location during various solstices (SS and WS) in influencing FPSRS performance was also underlined in this study. The HTC system proved to be a better option, especially at the lower value of θ offering encouraging possibilities for effectively capturing solar energy over several days.

Besides, it is observed from the Table 6.1 that ratio of area of STC/BRS would be higher than HTC/BRS, and that STC has a greater aperture area than HTC, the number of rays reaching the BRS in the case of STC is actually lower. This is due to a significant portion of the rays exiting the system because of its inability to redirect them to the BRS. Moreover, the number of LR type rays for STC is even more pronounced in the case of low solar altitude angles especially in WS condition. Conversely, in the case of HTC, its geometric advantages allow it to redirect most of the rays towards the BRS, resulting in fewer rays leaving the system. Furthermore, the number of case A and case B type rays is greater in the case of HTC. These factors play a crucial role in achieving the maximum value of η_{opt} for STSs. Overall, despite STC having a larger aperture area compared to HTC, the latter outperforms in terms of optical efficiency. This demonstrates the complex interplay between geometry and ray redirection in solar reflecting systems, highlighting the importance of optimizing

both factors for enhanced performance. However, in the following discussion, the comparative results from the OTC-based FPSRS are presented.

The results of the behavioural pattern of rays after being reflected from the reflectors of FPSRS, with both STC and OTC configurations, are presented in Fig. 6.14 for all the different classifications of the rays as discussed in Table 4.2. Firstly, the results for the RDP for case A type of rays are presented in Fig. 6.15 (a), where it is observed that STC exhibits a favourable response compared to OTC. The maximum value of the RDP in STC is 70%. The results of RDP for case B type of rays are shown in Fig. 4.15 (b), where there is no movement in RDP from 0° to 30° and from 150° to 180°. Additionally, a notably positive RDP is observed for the case of OTC when the value of θ ranges between 70° to 110°. A similar observation is noted for case C type of rays, but the RDP profile of STC does not show good results compared to OTC when θ is in the range of 15° to 40° and 140° to 165°, as seen from Fig. 6.15 (c). Yet, both types of configurations exhibit a similar RDP profile in the range of $40° < \theta < 140°$, and here too, OTC yields positive results compared to STC.

The results of case D type of rays are shown in Fig. 6.15 (d), and it is clearly indicated that OTC provides a better RDP profile than STC when the value of θ is between 30° to 150°. These findings suggest that the choice between STC and OTC configurations significantly impacts the performance of FPSRS in terms of ray distribution patterns, highlighting the importance of careful configuration selection in solar energy systems design and optimization. The results of the RDP in the case of E and F types of rays are depicted in Fig. 6.15 (e) and Fig. 6.15 (f), respectively. In the case of E and F types of rays, RDP is considered as the number of rays that left the system from the TIS relative to the number of rays that entered the system from the TIS. From Fig. 6.15 (e), it is observed that the number of rays leaving the system is highest for STC when the value of $0° < \theta < 45°$ and $130° < \theta < 180°$ for the case of E types of rays. Similarly, Fig. 6.15 (f) reveals that the number of rays leaving the system gradually decreases for both configurations when the value of $0° < \theta < 55°$ and $125° < \theta < 180°$. However, the overall observation suggests that OTC exhibits a better RDP profile than STC. This positively impacts the optical performance of the FPSRS. Therefore, for cases D, E, and F types of rays, the overall results of OTC are observed to be more favourable compared to STC. In conclusion, it can be stated that OTC offers a better and optimum RDP for the FPSRS compared to STC, highlighting the significance of optimizing the optical configuration for enhanced solar energy utilization.

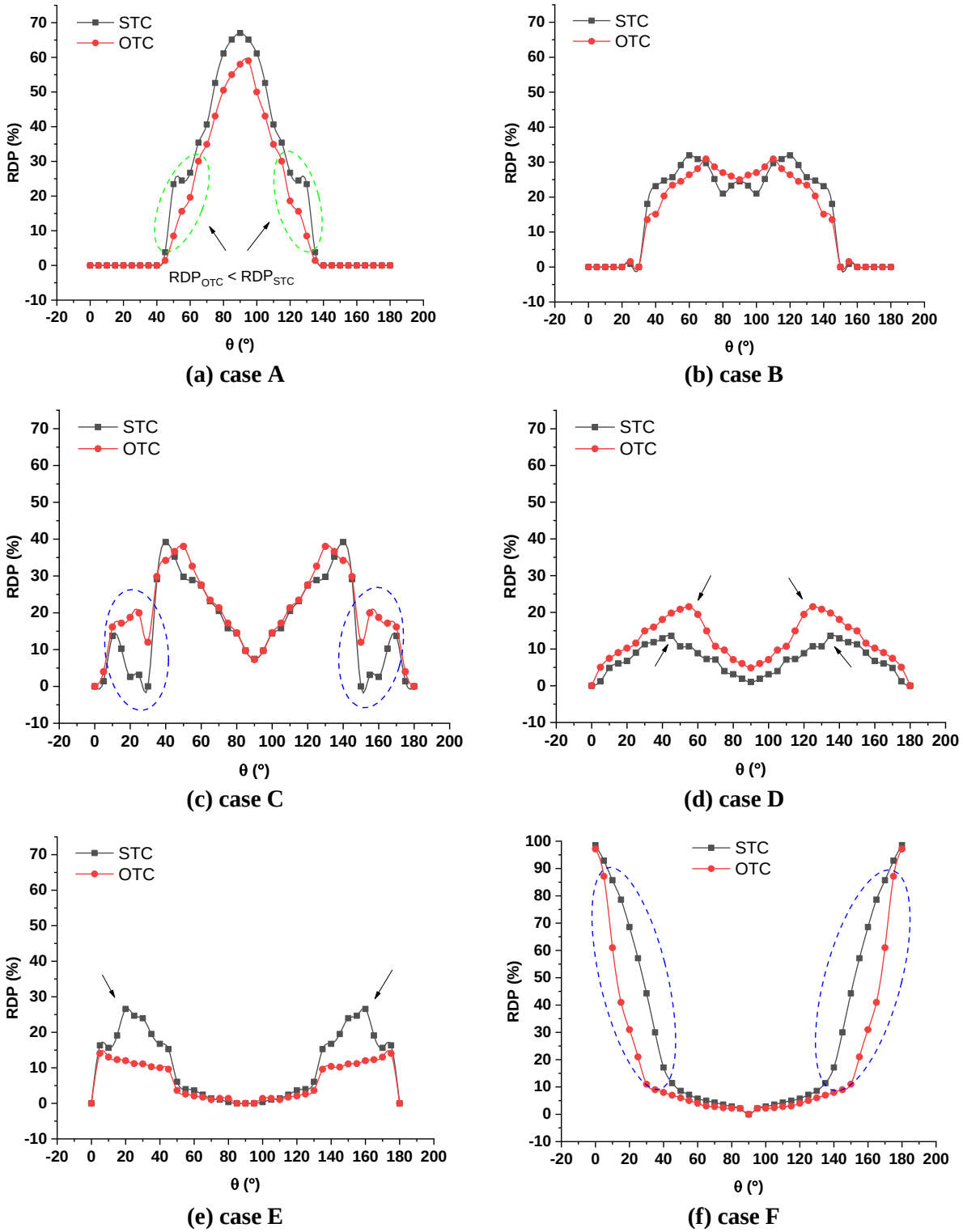

Fig. 6.15 Representation of the RDP for STC and OTC-based FPSRS for various values of θ as per the ray classification in Table 4.2.

The discussion above highlights that HTC and OTC demonstrate superior RDP compared to STC. However, to gain a better understanding of the optimal topology of the FPSRS, comparative results between OTC and HTC are presented in Fig. 6.16 for all similar classifications of rays. The RDP for different values of θ for the two configurations, HTC and OTC, is presented from Fig. 6.16 (a) to Fig. 6.16 (f) for all different types of rays from case A to case E. From the results, it is observed that there is a 12% higher RDP for case A type of rays for HTC compared to OTC. However, significant differences in the RDP values for both configurations are observed in cases B, D, and F. In the case of C type of rays, OTC exhibits better RDP results compared to HTC when θ ranges between 20° to 40° and from 120° to 140°. Similarly, for E type of rays, OTC demonstrates superior results when θ ranges from 10° to 40° and from 140° to 180°. Overall, major RDP values in favour of OTC are observed for cases C and E.

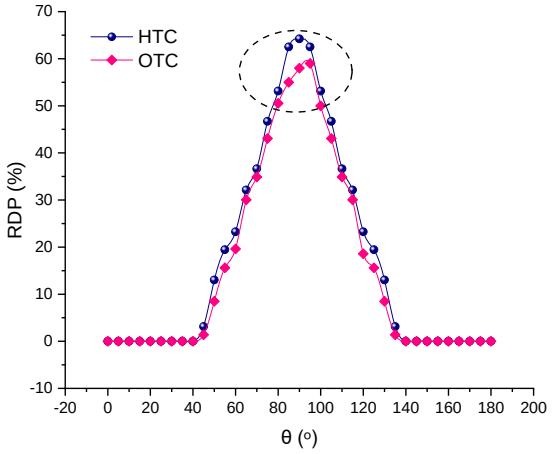

(a) case A

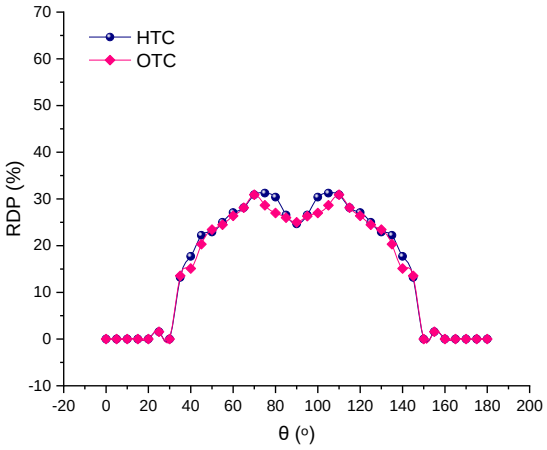

(b) case B

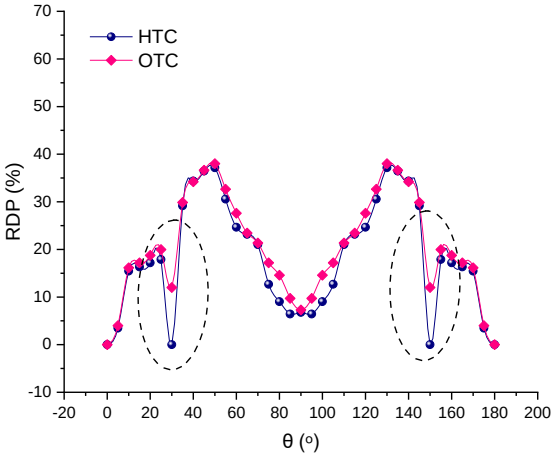

(c) case C

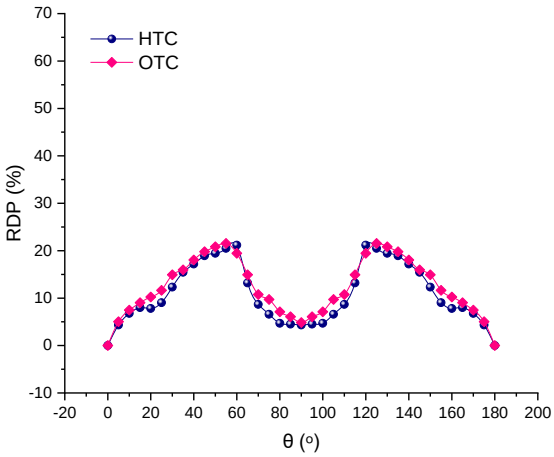

(d) case D

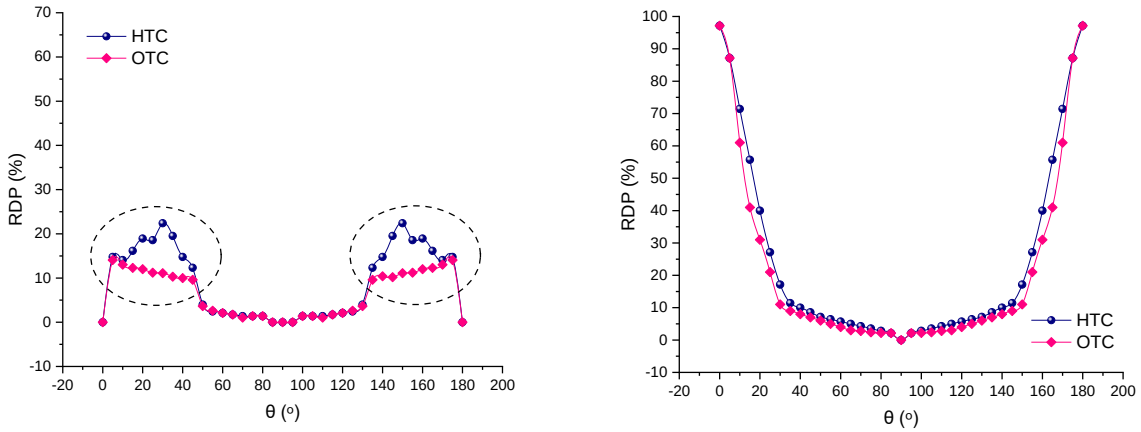

Fig. 6.16 Representation of the RDP for HTC and OTC-based FPSRS for various values of θ as per the ray classification in Table 4.2.

Additionally, Fig. 6.17 offers comprehensive comparative results with merging all the cases of rays (from A to F) for better understanding of the performance disparity between HTC and OTC. From Fig. 6.17 (a), it is discerned that OTC exhibits minor but consistent positive RDP values for cases A, B, and F in comparison to HTC. However, the transition from STC to HTC configuration shows a substantial average RDP increase of 18%, indicative of improved results. In contrast, Fig. 6.17 (b) highlights that transitioning from HTC to OTC configuration results in a more modest 8% increase in RDP compared to HTC. This underscores the nuanced impact of configuration changes on RDP. The subsequent discussion will explore into the optical performance of OTC-based FPSRS, initially focusing on both SS and WS scenarios, followed by an exploration across diverse urban cities in India. This will shed light on the efficacy and adaptability of such systems.

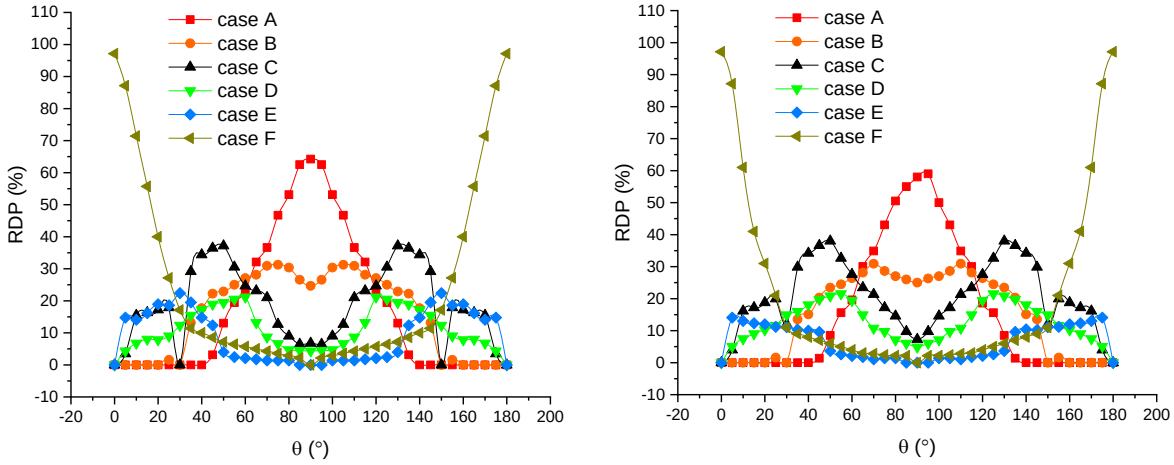

Fig. 6.17 Representation of the RDP for all the cases of the rays when (a) HTC based FPSRS and (b) OTC based FPSRS

The change in the value of η_{opt} for OTC-based FPSRS is shown in Fig. 6.18 (a) for SS and Fig. 6.18 (b) for WS solar radiation conditions. From the results, it is observed that the maximum value of η_{opt} is 87% and 75% in the cases of SS and WS conditions, respectively. A difference of 12% in η_{opt} between both conditions is noted when both conditions are at their peak optical performance, attributed to significant variation observed in the value of I_{TIS} for both SS and WS solar radiation conditions. Moreover, it is observed that from 6 AM to 1 PM, the change in the value of η_{opt} is almost similar in both solar radiation conditions. However, as the time changes from 1 PM to 6 PM, the value of η_{opt} does not follow the same decremented profile in both solar radiation conditions due to major variations in the value of α_L caused by extreme solar radiation conditions. Overall, the OTC yields notably better results compared to HTC and STC systems. Specifically, there is a 14% improvement in η_{opt} of OTC compared to STC, whereas this improvement is marginal in the case of HTC, with only a 9% difference. Hence, increasing the number of reflectors does not necessarily enhance optical input; instead, it only escalates the development cost of the system without a significant increase in optical performance. These findings underscore the importance of optimizing system design and reflector placement for maximizing efficiency.

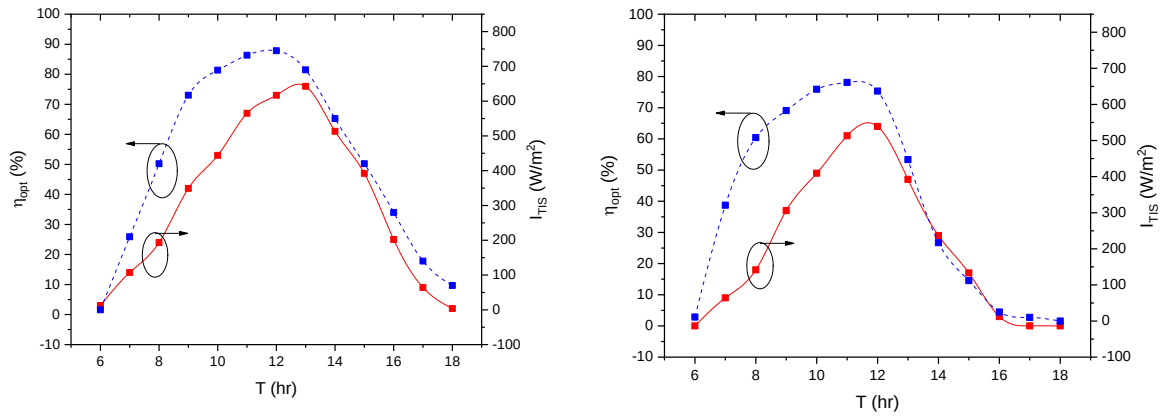

Fig. 6.18 Change in η_{opt} for OTC-based FPSRS under (a) SS and (b) WS solar radiation conditions

Hence, from the above discussion, it is observed that OTC performs better in extreme solar radiation conditions. Now, the optical efficiency of the OTC-based FPSRS for different cities of India is presented in Fig. 6.19 for the day of 21st June 2022, considered to be the SS of the year 2022 for all cities. The results of η_{opt} for four different cities in India, namely Delhi, Guwahati, Bangalore, and Gandhinagar, have been presented in Fig. 6.19 to understand the impact of different altitudes on the optical performance of the system. The input conditions for understanding the optical performance for the given cities have been shown in Appendix D. The Fig. D.1.2 representing the DNI radiation

received on the ground while Fig. D.2.2 shows the impact of $\alpha_L$on the receivable DNI on the surface for the chosen four cities of the India for the day of 21st June 2022.

From the results, it is observed that initially, there is no major variation, but as the day progresses, significant variations are observed. This is primarily attributed to the substantial changes in the DNI for different cities. The maximum values of η_{opt} for all four cities - Delhi, Guwahati, Bangalore, and Gandhinagar - are observed to be 93%, 91%, 89%, and 87%, respectively. Among these cities, Bengaluru and Gandhinagar exhibit the maximum and minimum values of η_{opt}, with a difference of about 7% at 12:30 PM. Moreover, Bengaluru exhibits the highest value ofη_{opt}, however the thermal performance does not increase proportionally with the optical performance enhancement. This disparity is attributed to the predominant participation of D-type rays. Conversely, Guwahati's optical performance remains relatively constant, with only a minor 3% change in the value of η_{opt} from 11:30 AM to 1:00 PM. This outcome emphasizes the significance of the OTC system in converting escaping rays into BRS, thus elevating the overall system performance.

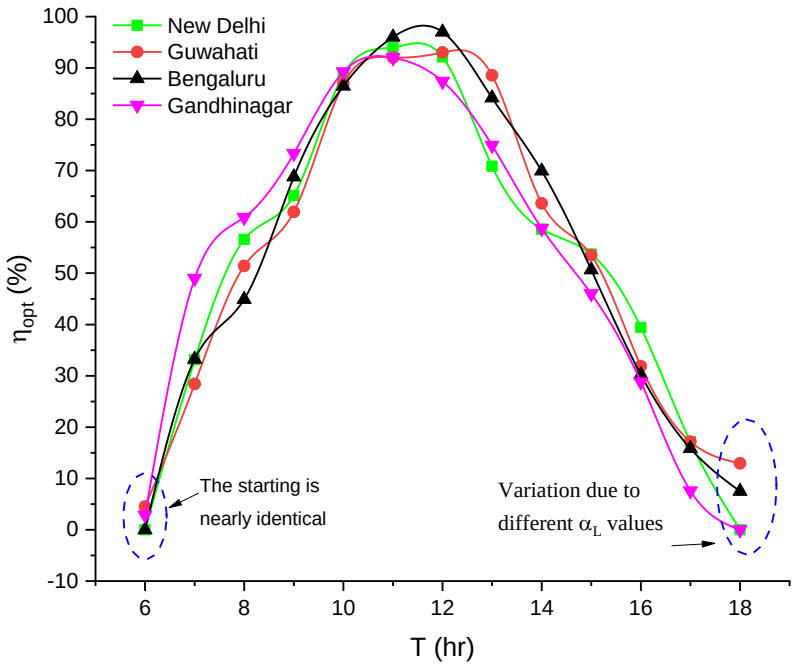

Fig. 6.19 Optical performance of OTC-based FPSRS for different cities of the India

Overall, the results suggest that utilizing OTC-based FPSRS is favourable in various scenarios, including extreme solar radiation conditions such as SS and WS. However, increasing the number of reflectors or transitioning to another configuration, such as an octagonal shape, does not necessarily improve optical input instead, it escalates system development costs without significantly enhancing optical performance. Similarly, reducing the number of reflectors from 4 to 3 diminishes optical performance due to multiple rays reflecting from the reflectors, particularly C and D types,

thereby reducing overall thermal performance. Additionally, these findings underscore the critical importance of optimizing system design and reflector placement to maximize efficiency. HTC demonstrates superiority over STC, while OTC outperforms HTC in all scenario. Despite the manufacturing limitations of complex OTC-based systems, their output surpasses these constraints, indicating the viability of utilizing OTC-based FPSRS in various scenarios for improved optical performance.

6.4 Summary

The present chapter numerically investigates the effect of different configurations on the optical performance of the FPSRS. Initially, methods for obtaining the most suitable H/B ratio are discussed, with a numerically analysed case study of STC-based FPSRS. Subsequently, the three chosen configurations STC, HTC, and OTC are evaluated for SS and WS solar radiation conditions, and the best configuration is selected for further study. The best selected OTC is analysed across different cities in India to understand its dynamic performance and improve the optical performance of the system under varying geometric conditions. Based on the results obtained, conclusions are drawn and discussed in the following,

- The findings suggest that the average RDP is at its best in SS solar radiation condition when H/B is 2, but the RDP is at its best in WS solar radiation condition when H/B is 1.52. Moreover, the value of Φ for the SS and WS solar radiation condition is 53° and 58°, respectively.
- The maximum attainable η_{opt} of the HTC was found to be 15% higher than that of the STC. This substantial difference underscores the geometrical advantages of the HTC. The higher value of η_{opt} is found in the case of HTC due to a greater participation of case of C and D types of rays compared to STC. The involvement values are 8% and 13% higher in the case of HTC. On the other hand, the STC showed increased engagement of case of E and F type of rays in the morning and evening hours. These elements together resulted in a lower overall RDP value for the STC than the HTC. It is clear from the overall findings that HTC outperforms STC in terms of performance.
- The numerical analysis of the OTC-based FPSRS suggests that it outperforms the STC system in terms of RDP for the different values of θ. A comparative study between HTC and OTC reveals that OTC achieves a higher value of η_{opt} than HTC under both SS and WS solar radiation conditions. Furthermore, despite its complex geometry, OTC demonstrates superior performance and effectively offsets its manufacturing costs. The numerical results from different cities for the OTC-based system indicate that the maximum value of η_{opt} is 93% for

Bengaluru, while the minimum value is 87% for Gandhinagar. However, overall, the OTC system performs better and exhibits superior optical performance across all cities.

Finally it is concluded that with utilizing OTC-based FPSRS proves beneficial in diverse scenarios, including extreme solar radiation conditions like SS and WS. However, increasing reflector numbers or transitioning to other configurations escalates costs without substantial optical performance gains. Optimizing system design and reflector placement is crucial for efficiency.